Differing Development of the Velocity Profiles of Three-Dimensional Turbulent Boundary Layers

H. Pfeil* and T. Amberg†
Institute for Thermal Turbomachines, Technische Hochschule Darmstadt (University), Darmstadt, Federal Republic of Germany

Nomenclature

c	= resultant mean velocity
c^+	= nondimensional resultant velocity, $= c/u_\tau$
F	= law of the wall function, Eq. (6), $= F(y^+\kappa,\eta)$
Re_δ	= Reynolds number based on boundary-layer thickness, $= U_\infty\delta/\nu$
u	= main-flow component of mean velocity in x direction
u_τ	= friction velocity, $=\sqrt{\tau_w/\rho}$
U_∞	= freestream velocity at the edge of the boundary layer
u_{1m}, w_m	= scaling velocities of the wake function, Eqs. (7) and (12)
$\Delta u_{1m}, \Delta w_m$	= differences of the scaling velocities of the wake function, Eqs. (7) and (12)
u^+	= nondimensional velocity component in x direction, $= u/u_{\tau x}$
w	= crossflow component of mean velocity in z direction
w^+	= nondimensional velocity component in z direction, $= w/u_{\tau z}$
X	= nondimensional, characteristic quantity, $= Re_\delta\omega\kappa = y^+\kappa\|_\delta$
x	= local coordinate aligned with the free streamline
y	= local coordinate normal to the wall
y^+	= nondimensional wall distance, $= yu_\tau/\nu$
z	= local coordinate normal to the free streamline
α	= angle of the free streamline
β	= cross flow angle
β_w	= angle of the wall shear stress
δ	= boundary-layer thickness
η	= nondimensional wall distance, $= y/\delta$
κ	= von Kármán constant, $= 0.41$
ν	= kinematic viscosity
ρ	= fluid density
τ_w	= wall shear stress
Φ_1	= wake function, Eq. (9)
Φ_2	= model function, Eq. (10)
ω	= nondimensional friction velocity, $= u_\tau/U_\infty$

Subscripts

C	= velocity component without the auxiliary distribution
i	= inner region, law of the wall
x,z	= in the respective coordinate direction
δ	= at the edge of the boundary layer

Received Sept. 14, 1988; revision received Jan. 12, 1989. Copyright © 1989 American Institute of Aeronautics and Astronautics, Inc. All rights reserved.

*Professor, Institute for Thermal Turbomachines.
†Research Engineer, Institute for Thermal Turbomachines.

I. Introduction

EXPERIMENTAL investigations of three-dimensional turbulent boundary-layer velocity profiles on infinite swept wings have shown that there is a good agreement of the main-flow component with the Coles model.[2] The streamlines are congruent along the infinite swept wing. If a suitable coordinate system is chosen, there exists a coordinate direction where the flowfield does not change, and the boundary-layer equations can be considerably simplified. The measurements of van den Berg and Elsenaar[1] are typical for this. In other cases the velocity profiles show deviations from Coles' profile model. Such experiments are, for instance, those of Dechow[3] and Müller.[5] In those cases the streamlines cannot be brought to coincidence by shifting them. The development along adjacent streamlines is different.

In order to make the different development of the velocity profiles clear, the mentioned measurements are evaluated by means of a velocity profile model. The evaluation indicates that the deviations of the main-flow component are definitely correlated with the deviations of the crossflow component from a basic distribution. All three data sets have in common that the three-dimensional boundary layer develops from a two-dimensional entrance flow and that the outer streamlines have no turning point. So called crossover profiles are not included. Only profiles upstream of separation are investigated.

II. Law of the Wall

Due to the small extent of the laminar sublayer, the crossflow angle $\beta = w/u$ differs only slightly from β_w. Therefore, to start with, it is allowed to assume that for this region

$$u_i = c_i\cos\beta_w,\quad w_i = c_i\sin\beta_w \tag{1}$$

and furthermore

$$u_{\tau x} = u_\tau\sqrt{\cos\beta_w},\quad u_{\tau z} = u_\tau\sqrt{\sin\beta_w} \tag{2}$$

In a similar way, $\kappa = 0.41$ can be split up into two components:

$$\kappa_x = \frac{\kappa}{\sqrt{\cos\beta_w}},\quad \kappa_z = \frac{\kappa}{\sqrt{\sin\beta_w}} \tag{3}$$

It follows that

$$y^+\kappa = y^+{}_x\kappa_x = y^+{}_z\kappa_z = \eta X \tag{4a}$$

$$X = Re_\delta\omega\kappa \tag{4b}$$

$$c_i{}^+\kappa = u_i{}^+\kappa_x = w_i{}^+\kappa_z \tag{5}$$

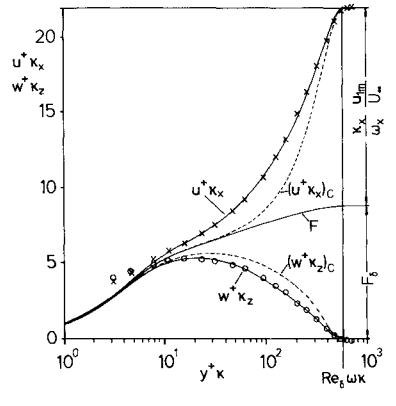

Fig. 1 Representation of the main-flow and crossflow components according to Eqs. (13) and (14) in comparison with measurements of Dechow[3] profile 7.

In order to describe the velocity distribution both in the viscous sublayer and in the region of transition toward the logarithmic law, a modified form of the law of the wall function of Pfeil and Sticksel[6] [also Pfeil and Müller[7] (see Fig. 1)] is assumed for the velocities $c_i{}^+$, $u_i{}^+$, and $w_i{}^+$:

$$c_i{}^+\kappa = u_i{}^+\kappa_x = w_i{}^+\kappa_z = F(y^+\kappa,\eta) = F(\eta X,\eta) = F$$
$$= \ln(1 + 0.5816y^+\kappa)$$
$$+ 3.4836$$
$$[1 - e^{-0.4541y^+\kappa}(1 + 0.3339y^+\kappa)] - \tfrac{1}{2}\eta^2 \qquad (6)$$

The corrective term $\frac{1}{2}\eta^2$ in Eq. (6) causes the derivative of the law of the wall function at the edge of the boundary layer to become zero.

III. Complete Velocity Profile Model

An evaluation of the measurements of van den Berg and Elsenaar[1] has shown that the main-flow component can be described by the Coles profile model,[2] whereas an auxiliary term is needed to describe the measurements of Dechow[3] and Müller.[5] The measurements of van den Berg and Elsenaar lead to a basic distribution of the crossflow component, but for the measurements of Dechow and Müller an auxiliary distribution is also required. The auxiliary distributions of the main-flow and cross-flow components are closely correlated. Both terms without the respective auxiliary distribution are labeled with the subscript C.

These considerations are laid down in the following formulas for the components of the complete velocity profile model:

Main-flow component:

$$\frac{u}{U_\infty} = \frac{\omega_x}{\kappa_x}F + \frac{u_{1m}}{U_\infty}(1 - \Phi_1) + \frac{\Delta u_{1m}}{U_\infty}\Phi_2 = \left(\frac{u}{U_\infty}\right)_C + \frac{\Delta u_{1m}}{U_\infty}\Phi_2 \qquad (7)$$

with

$$\frac{\omega_x}{\kappa_x} = \cos\beta_w\frac{\omega}{\kappa}$$

Crossflow component:

$$\frac{w}{U_\infty} = \frac{\omega_z}{\kappa_z}F - \frac{w_m}{U_\infty}(1 - \Phi_1) - \left(\frac{\omega_z}{\kappa_z}F_\delta - \frac{w_m}{U_\infty}\right)(1 - \Phi_1 + \Phi_2)$$
$$-\frac{\Delta w_m}{U_\infty}\Phi_2 = \left(\frac{w}{U_\infty}\right)_C - \frac{\Delta w_m}{U_\infty}\Phi_2 \qquad (8)$$

with

$$\frac{\omega_z}{\kappa_z} = \sin\beta_w\frac{\omega}{\kappa}$$

$$\Phi_1 = \cos^2\left(\frac{\pi}{2}\eta\right) \qquad (9)$$

$$\Phi_2 = \Phi_1 - e^{-10\eta^{1.25}} \qquad (10)$$

$$\frac{w_m}{U_\infty} = 2.4\sin\alpha\frac{u_{1m}}{U_\infty} \qquad (11)$$

$$\frac{\Delta w_m}{U_\infty} = 2.4\sin\alpha\frac{\Delta u_{1m}}{U_\infty} \qquad (12)$$

When Eq. (7) is multiplied by κ_x/ω_x and Eq. (8) by κ_z/ω_z, both components can be presented with a common law of the wall. That leads to the following relations:

Main-flow component :

$$u^+\kappa_x = F + \frac{\kappa_x}{\omega_x}\frac{u_{1m}}{U_\infty}(1 - \Phi_1) + \frac{\kappa_x}{\omega_x}\frac{\Delta u_{1m}}{U_\infty}\Phi_2 = (u^+\kappa_x)_C$$
$$+\frac{\kappa_x}{\omega_x}\frac{\Delta u_{1m}}{U_\infty}\Phi_2 \qquad (13)$$

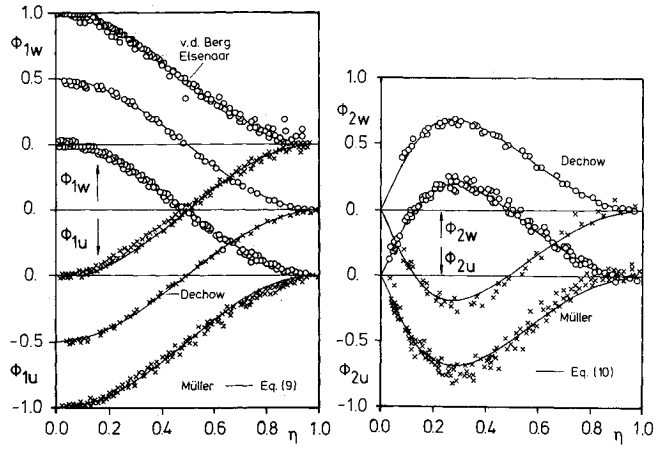

Fig. 2 Model functions Φ_1 and Φ_2 in comparison with experimental results.

Cross-flow component:

$$w^+\kappa_z = F - \frac{\kappa_z}{\omega_z}\frac{w_m}{U_\infty}(1 - \Phi_1) - \left(F_\delta - \frac{\kappa_z}{\omega_z}\frac{w_m}{U_\infty}\right)(1 - \Phi_1 + \Phi_2)$$
$$-\frac{\kappa_z}{\omega_z}\frac{\Delta w_m}{U_\infty}\Phi_2 = (w^+\kappa_z)_C - \frac{\kappa_z}{\omega_z}\frac{\Delta w_m}{U_\infty}\Phi_2 \qquad (14)$$

Both components of the profile model are shown together in Fig. 1 using this formulation.

IV. Comparison with Experimental Results

It is advantageous to evaluate each velocity profile of the measurement series investigated by means of the profile model according to Eqs. (13) and (14), because in a common representation such as in Fig. 1 both components have the same law of the wall. The resulting boundary-layer parameters δ, ω, β_w, α, and U_∞ are in a few cases slightly different from the data given by the authors. The parameter $\Delta u_{1m}/U_\infty$ and, therefore, according to Eq. (12), also $\Delta w_m/U_\infty$ is determined to obtain good agreement with the measured velocity profiles.

For further verification of the proposed model, Eqs. (7) and (8) are solved with respect to Φ_2 using the measured distributions of the main-flow and crossflow components and Φ_1, according to Eq. (9). Likewise, one can solve the same equations with respect to Φ_1 using Φ_2, according to Eq. (10). The results are shown in Fig. 2.

In Figs. 3 and 4, the measured distributions of the main-flow and crossflow components are shown in comparison with the model. Also shown are the distributions which result if one attempts to describe the main-flow component by the Coles profile model. This demonstrates that the crossflow component and its deviations are uniquely correlated with the main-flow component and its deviations by Eqs. (7), (8), (11), and (12). Independently of whether or not a $\Delta u_{1m}/U_\infty$ occurs, Eqs. (11) and (12) confirm the observation reported by Johnston[4] that in the outer region of the boundary layer there is

$$\frac{w}{U_\infty} \sim \sin\alpha\left(1 - \frac{u}{U_\infty}\right) \qquad (15)$$

This can easily be confirmed by comparing Eqs. (7) and (8). The velocity profiles measured by van den Berg and Elsenaar[1] on an infinite swept-wing model show no deviations from the Coles profile model, $\Delta u_{1m}/U_\infty = 0$, whereas the measurements of Dechow[3] and Müller[5] show deviations of the main-flow component that increase when β_w increases.

Many ways have been tried to find a dependence of $\Delta u_{1m}/U_\infty$ on other boundary-layer parameters. It appears that there exist some useful correlations between the measurements of

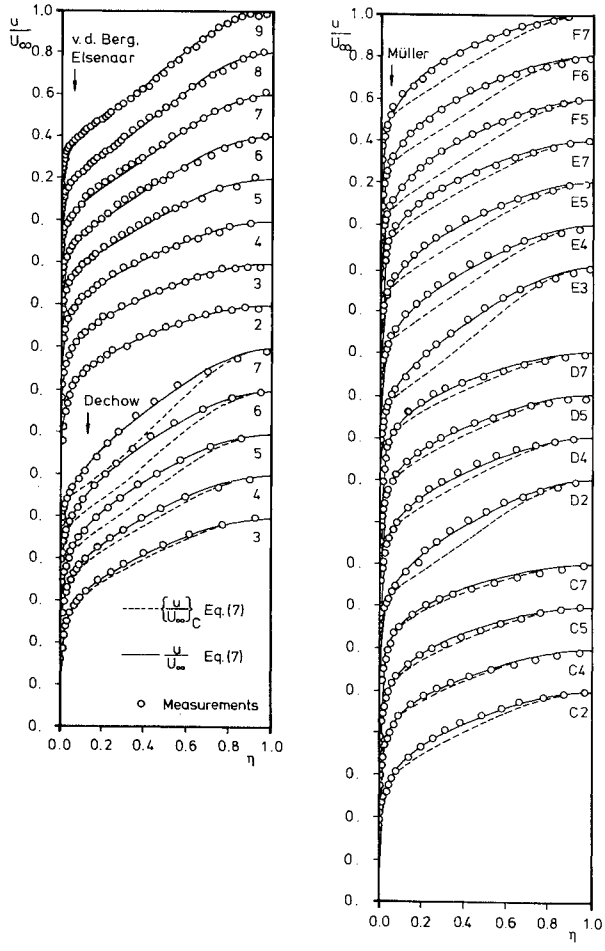

Fig. 3 Model for the main-flow component in comparison with experimental results.

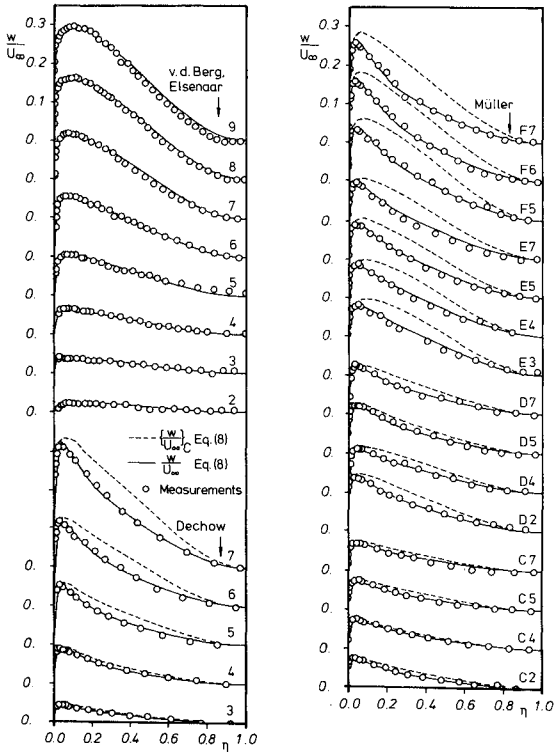

Fig. 4 Model for the crossflow component in comparison with experimental results.

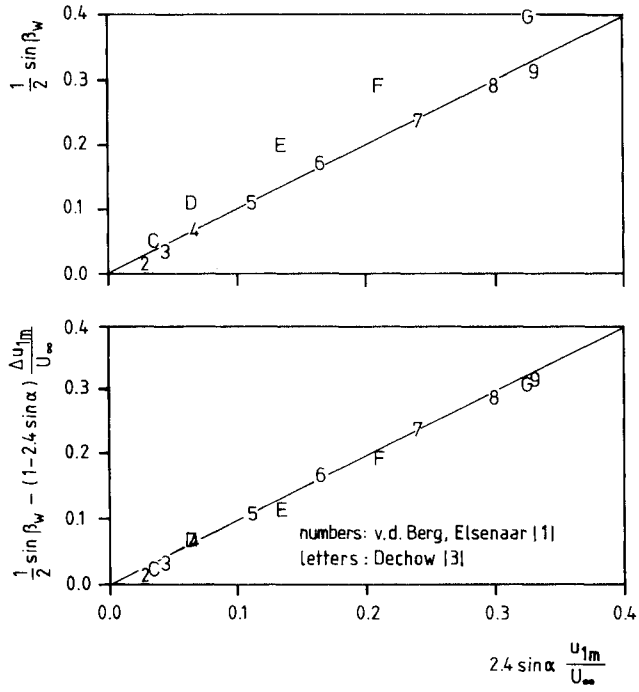

Fig. 5 Correlation between β_w, α, u_{1m}/U_∞ and $\Delta u_{1m}/U_\infty$ for the measurement series of van den Berg and Elsenaar[1] and Dechow.[3]

Refs. 1 and 3. For example, the following empirical correlation can be determined from both experiments (Fig. 5):

$$\frac{1}{2}\sin\beta_w - \frac{\Delta u_{1m}}{U_\infty}(1 - 2.4\sin\alpha) = 2.4\sin\alpha\frac{u_{1m}}{U_\infty} \qquad (16)$$

where $\Delta u_{1m}/U_\infty = 0$ is valid for the measurements of van den Berg and Elsenaar, as shown in Figs. 3 and 4.

Concerning the determination of $\Delta u_{1m}/U_\infty$, the measurements of Müller[5] do not fit into any of these correlations. Evaluation of other is measurements needed to show if it is possible to correlate $\Delta u_{1m}/U_\infty$ with boundary-layer parameters like Eq. (16). It may be necessary to include the gradients of these parameters or knowledge of the outer flowfield. It needs to be mentioned that there was a 5-mm trip wire at the beginning of Müller's[5] flow and that the measurements were taken at random points in a flowfield, in contrast to the other two sets of measurements which were taken along streamlines.

V. Conclusions

Analysis of three-dimensional turbulent boundary-layer data shows that even for small crossflow, i.e., for small angles β_w, the velocity profiles of the main-flow and crossflow components deviate distinctly from simple descriptive profile models when the streamlines are not congruent. These deviations can be well described by additional correlated distributions. Regarding the measurements of van den Berg and Elsenaar[1] and Dechow,[3] the coefficient $\Delta u_{1m}/U_\infty$, which appears in the additional distributions, is determined, for example, by Eq. (16) (see Fig. 5). The measurements of Müller[5] do not fit into this. Only evaluation of other measurements can show if the relation in Fig. 5 is universal.

Acknowledgment

The authors would like to thank the Deutsche Forschungsgemeinschaft (DFG) for supporting the work described here.

References

[1]van den Berg, B. and Elsenaar, A., "Measurements in a Three-Dimensional Incompressible Turbulent Boundary Layer in an Adverse Pressure Gradient under Infinite Swept-Wing Conditions," National Aerospace Lab., Amsterdam, the Netherlands, NLR TR 72092U, 1972.

[2]Coles, D., "The Law of the Wake in the Turbulent Boundary Layer," *Journal of Fluid Mechanics*, Vol. 1, Feb. 1956, pp. 191-226.
[3]Dechow, R., "Mittlere Geschwindigkeit und Reynoldscher Spannungstensor in der dreidimensionalen turbulenten Wandgrenzschicht vor einem stehenden Zylinder," Dissertation, Technische Hochschule Karlsruhe, Federal Republic of Germany, 1976.
[4]Johnston, J. P., "On the Three-Dimensional Turbulent Boundary Layer Generated by Secondary Flow," *Transactions of ASME, Journal of Basic Engineering*, Vol. 82, March 1960, pp. 233-248.
[5]Müller, U. R., "Messung von Reynoldsschen Spannungen und zeitlich gemittelten Geschwindigkeiten in einer dreidimensionalen Grenzschicht mit nichtverschwindenden Druckgradienten," Dissertation, Rheinisch Westfälische Technische Hochschule, Aachen, Federal Republic of Germany, March 1979.
[6]Pfeil, H. and Sticksel, W., "Influence of the Pressure Gradient on the Law of the Wall," *AIAA Journal*, Vol. 20, 1982, pp. 434-436.
[7]Pfeil, H. and Müller, T. "A Velocity Profile Model for Two-Dimensional Zero Pressure Gradient Transitional Boundary Layers," *AIAA Journal* (to be published).

Comparison of Iterative and Direct Solution Methods for Viscous Flow Problems

C. P. van Dam,* and M. Hafez†
University of California, Davis, Davis, California

Introduction

THE purpose of this study is to compare quantitatively several numerical solution techniques for solving two-dimensional viscous flow problems, including separated flows, at moderate to high Reynolds numbers. These solution techniques have various degrees of implicitness, and they are compared on the basis of convergence, CPU time, storage requirements, and solution accuracy. The stream-function (ψ) vorticity (ω) approach is used to formulate the partially parabolized Navier-Stokes (PPNS) equations that describe the two-dimensional incompressible flow. The PPNS equations are quite similar to the Navier-Stokes (NS) equations; streamwise diffusion is the only physical process neglected, and terms representing this diffusion are dropped from the NS equations. The governing equations are

$$\alpha\omega_t + (u\omega)_x + (v\omega)_y = (1/R)\omega_{yy} \tag{1}$$

$$-\omega = \psi_{xx} + \psi_{yy} \tag{2}$$

where the term $\alpha\omega_t$ represents an artificial time-dependent term, and the velocity $u = \psi_y$ and $v = -\psi_x$. At the solid wall, the no-slip boundary condition requires $u = 0$ and $v = 0$. For external flows $\omega = 0$ and $u = U(x)$ at the upper boundary. For internal flows the boundary conditions at the centerline of, e.g., a channel, are $\omega = 0$ and $\psi = \psi(x_0, y_c)$. At the inflow boundary ψ and ω are prescribed, whereas at the outflow boundary the PPNS equations are reduced to the boundary-layer equations by neglecting the ψ_{xx} term.

Received Aug. 10, 1987; revision received Nov. 4, 1988. Copyright © 1989 American Institute of Aeronautics and Astronautics, Inc. All rights reserved.

*Assistant Professor, Division of Aeronautical Science and Engineering, Department of Mechanical Engineering. Member AIAA.
†Professor, Division of Aeronautical Science and Engineering, Department of Mechanical Engineering. Associate Fellow AIAA.

Solution Techniques

Method I

The first solution technique employs a simple space marching procedure for the coupled stream-function and vorticity equations. Several authors have developed similar iterative methods to solve the NS equations or reduced equations.[1-5] The vorticity equation is linearized by lagging its coefficients. The resulting equation plus the stream-function equation are solved simultaneously for ω and ψ by using a line-relaxation procedure. Multiple global sweeps are required to obtain convergence. Centered differencing is applied for all terms except for the convective term $(u\omega)_x$. The problem of loss of diagonal dominance forces the use of an upwind differencing scheme for this term. Previously, the authors used a conservative first-order upwing differencing scheme for the convective term in the streamwise direction.[6] However, this scheme required excessively fine meshes to obtain grid-independent solutions. In this study the following second-order upwind differencing scheme is applied:

$$(u\omega)_x = \frac{3u_{i,j}\omega_{i,j} - 4u_{i-1,j}\omega_{i-1,j} + u_{i-2,j}\omega_{i-2,j}}{2\Delta x}$$

$$\text{if} \quad u_{i+\frac{1}{2},j} \geq 0 \quad \text{and} \quad u_{i-\frac{1}{2},j} \geq 0 \tag{3a}$$

$$(u\omega)_x = \frac{-3u_{i,j}\omega_{i,j} + 4u_{i-1,j}\omega_{i-1,j} - u_{i-2,j}\omega_{i-2,j}}{2\Delta x}$$

$$\text{if} \quad u_{i+\frac{1}{2},j} < 0 \quad \text{and} \quad u_{i-\frac{1}{2},j} < 0 \tag{3b}$$

$$(u\omega)_x = \frac{u_{i+1,j}\omega_{i+1,j} - u_{i-1,j}\omega_{i-1,j}}{2\Delta x}$$

$$\text{if} \quad u_{i+\frac{1}{2},j} \geq 0 \quad \text{and} \quad u_{i-\frac{1}{2},j} < 0 \tag{3c}$$

$$(u\omega)_x = \frac{-u_{i+2,j}\omega_{i+2,j} + 3u_{i+1,j}\omega_{i+1,j} - 3u_{i-1,j}\omega_{i-1,j} + u_{i-2,j}\omega_{i-2,j}}{2\Delta x}$$

$$\text{if} \quad u_{i+\frac{1}{2},j} < 0 \quad \text{and} \quad u_{i-\frac{1}{2},j} \geq 0 \tag{3d}$$

It can be shown that this scheme is conservative and that it is no more dissipative than a central differencing scheme. The resulting algebraic expressions have the following form:

$$a_1\psi_{i,j-1} + a_2\psi_{i,j} + a_3\omega_{i,j} + a_4\psi_{i,j+1} = a_5 \tag{4}$$

$$b_1\omega_{i,j-1} + b_2\omega_{i,j} + b_3\omega_{i,j+1} = b_4 \tag{5}$$

At each x location (i = const), the coefficients form a five-diagonal matrix. The solid wall and far-field boundary conditions are implemented as follows:

$$\psi_{i,1} = 0 \tag{6}$$

$$\omega_{i,1} = 2\left[\frac{\psi_{i,1} - \psi_{i,2}}{(\Delta y)^2}\right] \tag{7}$$

$$\omega_{i,N} = 0 \tag{8}$$

$$\frac{\psi_{i+1,N} + \psi_{i-1N}}{2(\Delta x)^2} - \psi_{i,N}\left[\frac{1}{(\Delta y)^2} + \frac{1}{(\Delta x)^2}\right] + \frac{\psi_{i,N-1}}{(\Delta y)^2}$$

$$= -\frac{\omega_{i,N}}{2} - \frac{U(x)}{\Delta y} \tag{9}$$

where M and N represent the number of grid points in the streamwise and normal direction, respectively. The system of equations is solved with a scalar pentadiagonal matrix solver. The convergence of this solution technique can be accelerated by the introduction of a relaxation parameter β for the stream-function equation.[4]